

Beyond Diagonal Reconfigurable Intelligent Surfaces: A Multi-Sector Mode Enabling Highly Directional Full-Space Wireless Coverage

Hongyu Li, *Student Member, IEEE*, Shanpu Shen, *Member, IEEE*, and Bruno Clerckx, *Fellow, IEEE*

Abstract—Reconfigurable intelligent surface (RIS) has gained much traction due to its potential to manipulate the propagation environment via nearly-passive reconfigurable elements. In our previous work, we have analyzed and proposed a beyond diagonal RIS (BD-RIS) model, which is not limited to traditional diagonal phase shift matrices, to unify different RIS modes/architectures. In this paper, we create a new branch of BD-RIS supporting a multi-sector mode. A multi-sector BD-RIS is modeled as multiple antennas connected to a multi-port group-connected reconfigurable impedance network. More specifically, antennas are divided into L ($L \geq 2$) sectors and arranged as a polygon prism with each sector covering $1/L$ space. Different from the recently introduced concept of intelligent omni-surface (or simultaneously transmitting and reflecting RIS), the multi-sector BD-RIS not only achieves a full-space coverage, but also has significant performance gains thanks to the highly directional beam of each sector. We derive the constraint of the multi-sector BD-RIS and the corresponding channel model taking into account the relationship between antenna beamwidth and gain. With the proposed model, we first derive the scaling law of the received signal power for a multi-sector BD-RIS-assisted single-user system. We then propose efficient beamforming design algorithms to maximize the sum-rate of the multi-sector BD-RIS-assisted multiuser system. Simulation results verify the effectiveness of the proposed design and demonstrate the performance enhancement of the proposed multi-sector BD-RIS.

Index Terms—Beyond diagonal reconfigurable intelligent surface (BD-RIS), full-space coverage, highly directional beam, multi-sector mode.

I. INTRODUCTION

The forthcoming next-generation 6G is expected to address 5G drawbacks, improve existing techniques, and lead new technological trends [1]. Reconfigurable intelligent surface (RIS) is regarded as one of the promising techniques which will drive the 6G architectural evolution [2]. The RIS, usually consisting of multiple nearly-passive reconfigurable elements whose amplitudes and/or phases can be flexibly adjusted, enables adaptive manipulations of the scattered signals [3]. The “nearly-passive” and “reconfigurable” characteristics of the RIS show its potential to shape the propagation environment as intended in an easily deployed way with a reduced cost, power consumption, and weight [4].

Manuscript received; (Corresponding author: Shanpu Shen).

H. Li and B. Clerckx are with the Department of Electrical and Electronic Engineering, Imperial College London, London SW7 2AZ, U.K. (email: {c.li21,b.clerckx}@imperial.ac.uk).

S. Shen is with the Department of Electronic and Computer Engineering, The Hong Kong University of Science and Technology, Clear Water Bay, Kowloon, Hong Kong (email: sshenaa@connect.ust.hk).

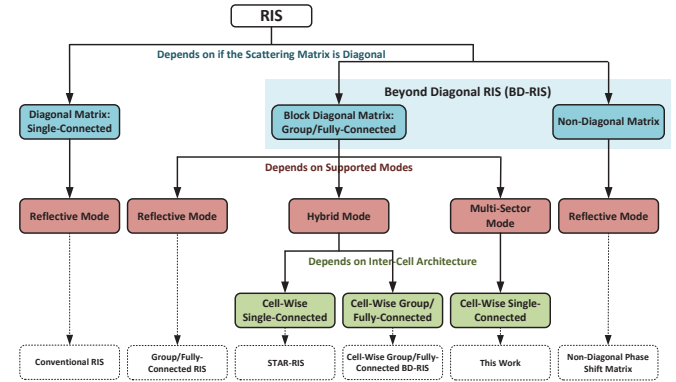


Fig. 1. RIS classification tree.

Given the appealing potential of RIS, extensive work [5]–[27] has been devoted to modeling and optimizations for RIS-assisted systems. To clearly classify the existing works, we categorize RIS, according to the mathematical characteristic of the scattering matrix of RIS, into diagonal RIS where the scattering matrix is diagonal, and beyond diagonal RIS (BD-RIS) where the scattering matrix is not restricted to be diagonal, as shown in Fig. 1. In the following, we will classify the existing studies [5]–[27] by mapping them to different branches in Fig. 1.

For conventional RIS [5]–[21], each element is connected to its own reconfigurable load, but is disconnected from other elements. Therefore, the scattering matrix of conventional RIS [5]–[21] is modeled as a simple *diagonal phase shift matrix*. This kind of RIS can only reflect signals from one side of the RIS towards the receiver, and thus only supports the reflective mode. With the diagonal RIS, beamforming designs focusing on different metrics, such as rate maximization [5], [6], energy-efficiency maximization [7], power minimization [8], [9], and max-min fairness [10], have been developed for various RIS-aided wireless communication systems with continuous phase shifts [5], [7]–[10] and discrete phase shifts [6], [9]. In addition, the integration of RIS and other techniques has also been widely investigated, such as rate-splitting multiple access (RSMA) [11], wireless power transfer (WPT) [12], simultaneous wireless information and power transfer (SWIPT) [13], integrated sensing and communication (ISAC) [14], cognitive radio [15], and index modulation [16]. The aforementioned works [5]–[16] assume an ideal RIS phase shift model where its diagonal elements have unit modulus, while only a few results focus on the modeling of RIS

accounting for the lumped inductance and capacitance [17]–[19]. In addition, the near- and far-field free-space path loss models for RIS-aided systems are also theoretically derived [20], [21] and experimentally verified [21].

Different from traditional RISs having diagonal scattering matrices, BD-RISs have scattering matrices not limited to diagonal ones, which can provide more flexible beam management. In existing works, there are two branches belonging to BD-RIS supporting the reflective mode, as shown in Fig. 1. On one hand, [22] gets deeper into the essence of RIS and for the first time model the RIS based on scattering parameter network. They go beyond diagonal phase shift models [5]–[21] (with a single-connected architecture), and propose more general group/fully-connected architectures with block-diagonal matrices. Different from the single-connected architecture that only adjusts the phase shifts of incident waves, the group/fully-connected architectures enable both amplitude and phase shift manipulations, therefore providing additional beam control flexibility. Based on the proposed architectures in [22], the authors in [23] designed codebooks for group/fully-connected RIS with discrete-value impedance networks. Results show that the size of the codebook needed in fully-connected RIS can be significantly reduced compared to that in conventional RIS, highlighting the hardware realizing feasibility of fully-connected RIS. On the other hand, [24] proposes another novel RIS architecture under the BD-RIS branch, where the signal impinging on one reconfigurable element can be reflected from another one, yielding a non-diagonal phase shift matrix. Results show that the performance achieved by this non-diagonal RIS can be better than that achieved by the group-connected RIS, and close to that achieved by the fully-connected RIS.

The limitation of the RIS models used in [5]–[24] is that incident signals can only be reflected to one side of the RIS, which means both the transmitter and the receiver should be deployed in the same side of the RIS and thus half-space is out of the coverage of the RIS. To address this issue, the concept of simultaneously transmitting and reflecting RIS (STAR-RIS) [25] or intelligent omni-surface (IOS) [26] has been introduced recently. The STAR-RIS is a dual-functional device enabling signal manipulations of both reflection and transmission, that is supporting the hybrid reflective and transmissive mode, to achieve full-space coverage. However, there are two limitations of the model utilized in [25], [26]: *i*) The STAR-RIS is lack of physical meaning. *ii*) The STAR-RIS is only an application of group-connected reconfigurable impedance network [22] as illustrated in Fig. 1, while different architectures of BD-RIS supporting the hybrid mode have not been investigated.

To fill in the research blanks of BD-RIS under the hybrid mode, in our recent work [27], we analyze and propose a general BD-RIS model unifying reflective/transmissive/hybrid modes and single/fully/group-connected architectures. Specifically, we first show that STAR-RIS is a specific application of group-connected reconfigurable impedance network with group size equal to 2. Then we go beyond STAR-RIS and create a novel branch, also belonging to BD-RIS supporting the hybrid model, but with more general group/fully-connected architectures, as shown in Fig. 1. Results show that the proposed architectures can always achieve better performance

than STAR-RIS regardless of channel fading conditions.

To further enhance RIS performance, in this work, we propose a novel multi-sector BD-RIS, which is shown as a branch of BD-RIS in Fig. 1, to provide pronounced performance gains while realizing full-space communications. More specifically, we have the following contributions.

First, we, for the first time, propose a multi-sector BD-RIS, which is modeled as a multiple-sector polygonal prism as shown in Fig. 2(a). The proposed model is general enough to include STAR-RIS/IOS as a special instance and achieve full-space coverage, but provides significant performance enhancements compared to IOS/STAR-RIS. With full-space coverage, highly directional beams, and adaptive structures (based on different numbers of sectors), the multi-sector BD-RIS can be flexibly deployed into various situations and is particularly favorable to higher-frequency millimeter wave/Terahertz communications and cell-free networks.

Second, we derive the constraints of the multi-sector BD-RIS when its reconfigurable elements have either continuous amplitudes/phase shifts or discrete values selected from finite codebooks. We also derive the corresponding channel model by taking the relationship between the beamwidth and the antenna gain into consideration.

Third, with the proposed model, we derive the scaling law of the received signal power as a function of the number of sectors for a multi-sector BD-RIS-assisted single user single-input single-output (SU-SISO) system to show the benefits of using multi-sector BD-RIS.

Fourth, we apply the proposed multi-sector BD-RIS in multiuser multiple-input single-output (MU-MISO) systems. Specifically, we propose efficient algorithms to maximize the sum-rate performance of the multi-sector BD-RIS-assisted MU-MISO system. We first derive the closed-form solution of the multi-sector BD-RIS when its scattering matrix has continuous values. Then we quantize the continuous solution, together with some adjustments, to obtain the discrete solution.

Fifth, we evaluate the sum-rate performance of the multi-sector BD-RIS-aided MU-MISO system. Numerical results show that with the same sum-rate performance requirement, the number of antennas for the whole multi-sector BD-RIS can be reduced by increasing the number of sectors. In addition, the resolution of the finite codebooks for the multi-sector BD-RIS with discrete values can be reduced with increasing number of sectors, which is beneficial for controlling cost for practical RIS realizations.

Organization: Section II proposes a novel multi-sector BD-RIS model and derives the corresponding channel model. Section III lists potential applications of the multi-sector BD-RIS. Section IV derives the scaling law for the multi-sector BD-RIS-assisted SU-SISO system. Section V provides the beamforming design for the multi-sector BD-RIS-assisted MU-MISO system. Section VI evaluates the performance of the proposed design and Section VII concludes this work.

Notations: Boldface lower- and upper-case letters indicate column vectors and matrices, respectively. \mathbb{C} , \mathbb{R} , and \mathbb{Z} denote the set of complex numbers, real numbers, and integers, respectively. $\mathbb{E}\{\cdot\}$ represents statistical expectation. $(\cdot)^*$, $(\cdot)^T$, $(\cdot)^H$, and $(\cdot)^{-1}$ denote the conjugate, transpose, conjugate-

transpose operations, and inversion, respectively. $\mathcal{CN}(0, \sigma^2)$ denotes the circularly symmetric complex Gaussian distribution with zero mean and covariance σ^2 . $\mathcal{U}(a, b)$ denotes the continuous uniform distribution with boundaries a and b . $\Re\{\cdot\}$ denotes the real part of a complex number. \mathbf{I}_L indicates an $L \times L$ identity matrix. $\mathbf{0}$ denotes an all-zero matrix. $\|\mathbf{A}\|_F$ denotes the Frobenius norm of matrix \mathbf{A} . $|a|$ denotes the norm of variable a . $\text{diag}(\cdot)$ denotes a diagonal matrix. $j = \sqrt{-1}$ denotes imaginary unit. $\text{Tr}\{\cdot\}$ denotes the summation of diagonal elements of a matrix. Finally, $[\mathbf{A}]_{i,:}$, $[\mathbf{A}]_{:,j}$, $[\mathbf{a}]_i$ denote the i -th row, the j -th column, the (i, j) -th element of matrix \mathbf{A} , and the i -th element of vector \mathbf{a} , respectively.

II. MULTI-SECTOR BD-RIS MODEL

In this section, we propose the multi-sector BD-RIS-assisted communication model based on [22], [28], and specify the channel model based on antenna theory [29].

We consider a general wireless communication system consisting of an N -antenna transmitter, K multi-antenna users, each of which has N_k antennas, and an M -cell RIS. Denote $\mathcal{N} = \{1, \dots, N\}$, $\mathcal{K} = \{1, \dots, K\}$, and $\mathcal{M} = \{1, \dots, M\}$ as the set of indices of transmitting antennas, users, and cells, respectively. Each cell in this RIS consists of L antennas, $L \geq 2$. Particularly, cell m contains antennas belonging to the set $\mathcal{L}_m = \{m, M+m, \dots, (L-1)M+m\}$, $\forall m \in \mathcal{M}$. Therefore, the M -cell RIS is modeled as LM antennas connected to an ML -port reconfigurable impedance network [22]. The channel between the transmitter and user k without mismatching and mutual coupling is [22]

$$\mathbf{H}_k = \mathbf{H}_{\text{UT},k} + \overline{\mathbf{H}}_{\text{UI},k} \Phi \overline{\mathbf{H}}_{\text{IT}}, \forall k \in \mathcal{K}, \quad (1)$$

where $\mathbf{H}_{\text{UT},k} \in \mathbb{C}^{N_k \times N}$ is the channel matrix for the transmitter-user link, $\overline{\mathbf{H}}_{\text{UI},k} \in \mathbb{C}^{N_k \times LM}$, $\forall k \in \mathcal{K}$ and $\overline{\mathbf{H}}_{\text{IT}} \in \mathbb{C}^{LM \times N}$ are channel matrices for the transmitter-RIS-user link. $\Phi \in \mathbb{C}^{LM \times LM}$ is the scattering matrix of the LM -port reconfigurable impedance network satisfying [29]

$$\Phi^H \Phi = \mathbf{I}_{LM}, \quad (2)$$

when the LM -port reconfigurable impedance network is lossless. More details can be found in [22], [29].

The channel model (1) and the constraint for an M -cell RIS (2) are general expressions regardless of architectures of RIS, spatial arrangements and radiation pattern of RIS antenna elements. In the following, we will propose a novel multi-sector BD-RIS model and derive corresponding multi-sector BD-RIS-assisted channel model by specifying the spatial arrangement of RIS antenna elements and the architecture of the RIS. To this end, we first make the following two assumptions.

Assumption 1. Each antenna of the RIS has a uni-directional radiation pattern with beamwidth $2\pi/L$.

Assumption 2. The L antennas in each cell are respectively placed at the side of the polygon such that each antenna covers $1/L$ space, as illustrated in Fig. 2 (b).

Based on Assumptions 1 and 2, we divide the M -cell RIS into L sectors. Specifically, sector l covers $1/L$ space

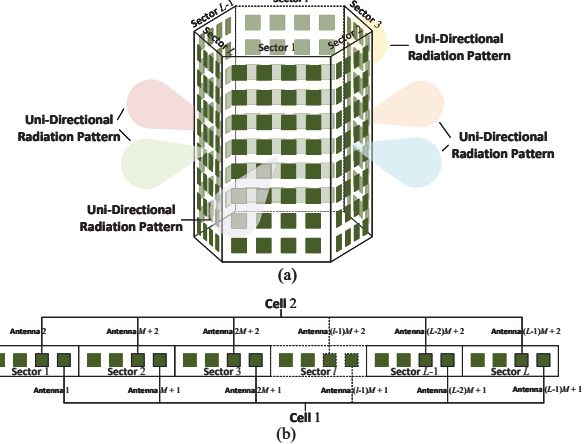


Fig. 2. (a) A multi-sector BD-RIS with LM uni-directional antennas modeled as an L -sector polygon. (b) Illustration of cells 1 and 2 taking the first row of the multi-sector BD-RIS (stretched in a straight line) as an example.

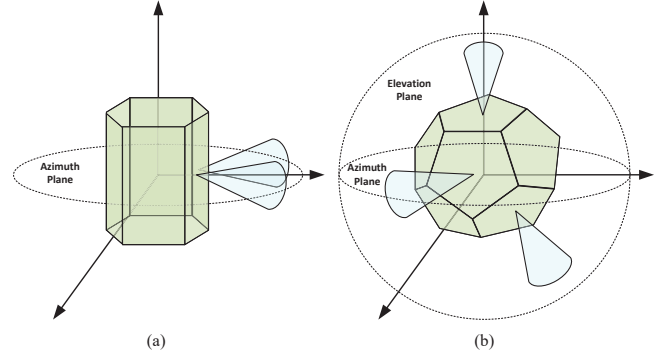


Fig. 3. Multi-sector BD-RIS modeled as (a) a 2D polygon with 6 sectors and (b) a 3D polygon with 12 sectors.

containing M antennas, each of which belongs to $\mathcal{M}_l = \{(l-1)M+1, \dots, lM\}$, $\forall l \in \mathcal{L} = \{1, \dots, L\}$. The M -cell RIS is thus modeled as a polygon with L -sectors, which is referred to as multi-sector BD-RIS as shown in Fig. 2.

Remark 1. In this work, we focus on a 2D polygon for illustration and tractability. In Fig. 3(a), we provide a simple example when the multi-sector BD-RIS is modeled as a 2D polygon with 6 sectors. In this case, we assume the multi-sector BD-RIS has a 2D horizontal coverage at the azimuth plane. However, the concept is also applicable to 3D polygon where antennas are placed on a “sphere”. For ease of understanding, we provide an example when the multi-sector BD-RIS is modeled as a 3D polygon with 12 sectors in Fig. 3(b). In this case, the multi-sector BD-RIS enables a 3D full-space coverage.

With Assumptions 1 and 2, we can partition channel (1) as

$$\begin{aligned} \mathbf{H}_k &= \mathbf{H}_{\text{UT},k} + [\overline{\mathbf{H}}_{\text{UI},k,1} \ \overline{\mathbf{H}}_{\text{UI},k,2} \ \dots \ \overline{\mathbf{H}}_{\text{UI},k,L}] \\ &\quad \times \begin{bmatrix} \Phi_{1,1} & \Phi_{1,2} & \dots & \Phi_{1,L} \\ \Phi_{2,1} & \Phi_{2,2} & \dots & \Phi_{2,L} \\ \vdots & \vdots & \ddots & \vdots \\ \Phi_{L,1} & \Phi_{L,2} & \dots & \Phi_{L,L} \end{bmatrix} \begin{bmatrix} \overline{\mathbf{H}}_{\text{IT},1} \\ \overline{\mathbf{H}}_{\text{IT},2} \\ \vdots \\ \overline{\mathbf{H}}_{\text{IT},L} \end{bmatrix} \\ &= \mathbf{H}_{\text{UT},k} + \sum_{l \in \mathcal{L}} \sum_{l' \in \mathcal{L}} \overline{\mathbf{H}}_{\text{UI},k,l} \Phi_{l,l'} \overline{\mathbf{H}}_{\text{IT},l'}, \forall k \in \mathcal{K}, \end{aligned} \quad (3)$$

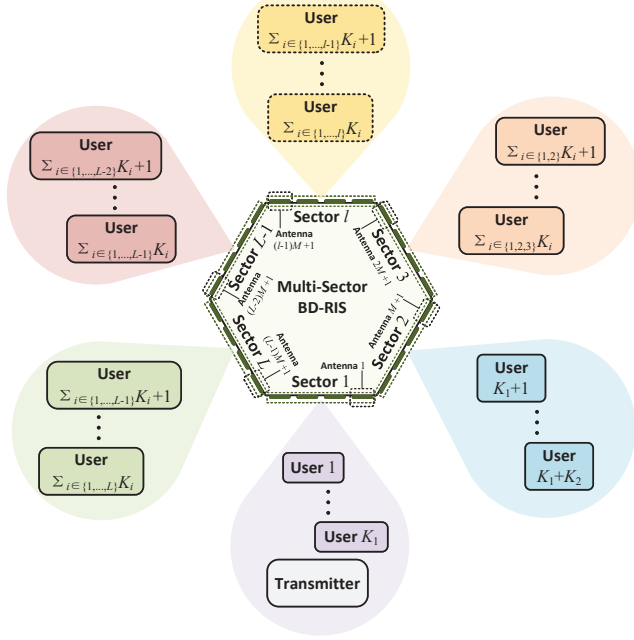


Fig. 4. Top view for the locations of the M -cell multi-sector BD-RIS partitioning the whole space into L sectors, the transmitter, and multiple users.

where $\bar{\mathbf{H}}_{\text{UI},k,l} = [\bar{\mathbf{H}}_{\text{UI},k}]_{:, (l-1)M+1: lM} \in \mathbb{C}^{N_k \times M}$, and $\bar{\mathbf{H}}_{\text{IT},l} = [\bar{\mathbf{H}}_{\text{IT}}]_{(l-1)M+1: lM, :} \in \mathbb{C}^{M \times N}$, $\forall k \in \mathcal{K}$, $\forall l \in \mathcal{L}$ are channels between sector l of the multi-sector BD-RIS and user k , and between the transmitter and sector l , respectively. $\Phi_{l,l'} = [\Phi]_{(l-1)M+1: lM, (l'-1)M+1: l'M} \in \mathbb{C}^{M \times M}$, $\forall l, l' \in \mathcal{L}$. To derive the multi-sector BD-RIS-assisted channel model, we further make the following assumption.

Assumption 3. *The transmitter and K_1 users with $\mathcal{K}_1 = \{1, \dots, K_1\}$, $0 < K_1 < K$ are located within the coverage of sector 1 of the multi-sector BD-RIS; K_l users with $\mathcal{K}_l = \{\sum_{i \in \{1, \dots, l-1\}} K_i + 1, \dots, \sum_{i \in \{1, \dots, l\}} K_i\}$, $0 < K_l < K$ are located within the coverage of sector l of the multi-sector BD-RIS, $\forall l \in \mathcal{L}, l \neq 1$, as illustrated in Fig. 4.*

Based on Assumptions 1-3, we can deduce two corollaries.

Corollary 1. *The transmitter is out of the coverage of the uni-directional radiation pattern of sector l of the multi-sector BD-RIS, $\forall l \in \mathcal{L}, l \neq 1$, that is $\bar{\mathbf{H}}_{\text{IT},l} = \mathbf{0}$, $\forall l \in \mathcal{L}, l \neq 1$.*

Corollary 2. *The users in \mathcal{K}'_l are out of the coverage of the uni-directional radiation pattern of sector l of the multi-sector BD-RIS, $\forall l \neq l'$, that is $\bar{\mathbf{H}}_{\text{UI},k,l} = \mathbf{0}$, $\forall k \in \mathcal{K}_{l'}$, $\forall l \neq l', \forall l' \in \mathcal{L}$.*

With Corollaries 1 and 2, we can simplify (3) as

$$\mathbf{H}_k = \mathbf{H}_{\text{UT},k} + \bar{\mathbf{H}}_{\text{UI},k,l} \Phi_{l,1} \bar{\mathbf{H}}_{\text{IT},1}, \forall k \in \mathcal{K}_l, \forall l \in \mathcal{L}. \quad (4)$$

For simplicity, we use auxiliary notations $\mathbf{H}_{\text{UI},k} = \bar{\mathbf{H}}_{\text{UI},k,l}$, $\Phi_l = \Phi_{l,1}$, $\mathbf{H}_{\text{IT}} = \bar{\mathbf{H}}_{\text{IT},1}$, $\forall k \in \mathcal{K}_l$, $\forall l \in \mathcal{L}$. We also ignore the channel from the transmitter to the receiver ($\mathbf{H}_{\text{UT},k} = \mathbf{0}$, $\forall k \in \mathcal{K}$). Then we can rewrite the simplified channel (4) as

$$\mathbf{H}_k = \mathbf{H}_{\text{UI},k} \Phi_l \mathbf{H}_{\text{IT}}, \forall k \in \mathcal{K}_l, \forall l \in \mathcal{L}. \quad (5)$$

TABLE I
THREE ARCHITECTURES OF MULTI-SECTOR BD-RIS

(Cell-Wise) Architectures	Constraint
Single-Connected	$\Phi_l = \text{diag}(\phi_{(l-1)M+1}, \dots, \phi_{lM})$ $\sum_{i \in \mathcal{L}_m} \phi_i ^2 = 1, \forall m \in \mathcal{M}$
Group-Connected [†]	$\Phi_l = \text{blkdiag}(\Phi_{l,1}, \dots, \Phi_{l,G})$ $\sum_{\forall l \in \mathcal{L}} \Phi_{l,g}^H \Phi_{l,g} = \mathbf{I}_M, \forall g \in \mathcal{G}$
Fully-Connected	$\sum_{\forall l \in \mathcal{L}} \Phi_l^H \Phi_l = \mathbf{I}_M$

[†] G is the number of groups [27]. $\mathcal{G} = \{1, \dots, G\}$, $\bar{M} = M/G$.

According to the general constraint (2), the constraint of matrices Φ_l , $\forall l \in \mathcal{L}$ of the multi-sector BD-RIS becomes

$$\sum_{\forall l \in \mathcal{L}} \Phi_l^H \Phi_l = \mathbf{I}_M. \quad (6)$$

Now we establish the multi-sector BD-RIS-assisted communication model (6) and (5). In the following subsections, we will show the specific descriptions of matrices Φ_l , $\forall l \in \mathcal{L}$ when the cell-wise single-connected architecture is applied and channels \mathbf{H}_k , $\forall k \in \mathcal{K}$ including the impact of antenna gain.

A. Cell-Wise Single-Connected Multi-Sector BD-RIS

In this work, we assume the multi-sector BD-RIS has a cell-wise single-connected architecture, that is, different RIS cells are not connected to each other. Similar to [27], with different inter-cell circuit topologies, the multi-sector BD-RIS can also have different architectures, namely, cell-wise single/group/fully-connected architectures, which are summarized in Table I. The cell-wise group/fully-connected architectures can provide higher performance gains thanks to the more general constraints as shown in Table I, but at the expense of higher circuit topology complexity. Here we focus only on cell-wise single-connected multi-sector BD-RIS and investigating cell-wise group/fully-connected architectures is left for future work. In the cell-wise single-connected case, Φ_l , $\forall l \in \mathcal{L}$ can be modeled as diagonal matrices:

$$\Phi_l = \text{diag}(\phi_{(l-1)M+1}, \dots, \phi_{lM}), \forall l \in \mathcal{L}, \quad (7)$$

and constraint (6) becomes

$$\sum_{i \in \mathcal{L}_m} |\phi_i|^2 = 1, \forall m \in \mathcal{M}. \quad (8)$$

Remark 2. *We should clarify here that the proposed cell-wise single-connected multi-sector BD-RIS is an application of group-connected reconfigurable impedance network with group size equal to L . When antennas with different spatial arrangements are connected to the same reconfigurable impedance network, we have different kinds of RIS models. In Fig. 5 we provide a simple example to facilitate understanding. We can easily observe from Fig. 5 that the circuit topology of the impedance network for a 2-cell 4-sector BD-RIS with cell-wise single-connected architecture is exactly the same as that for an 8-element group-connected RIS with group size equal to 4 [22]. The difference is that antennas within each cell of the multi-sector BD-RIS are placed at the side of the polygon, while antennas of the RIS in [22] are placed towards one direction. Therefore, the freedom induced by the*

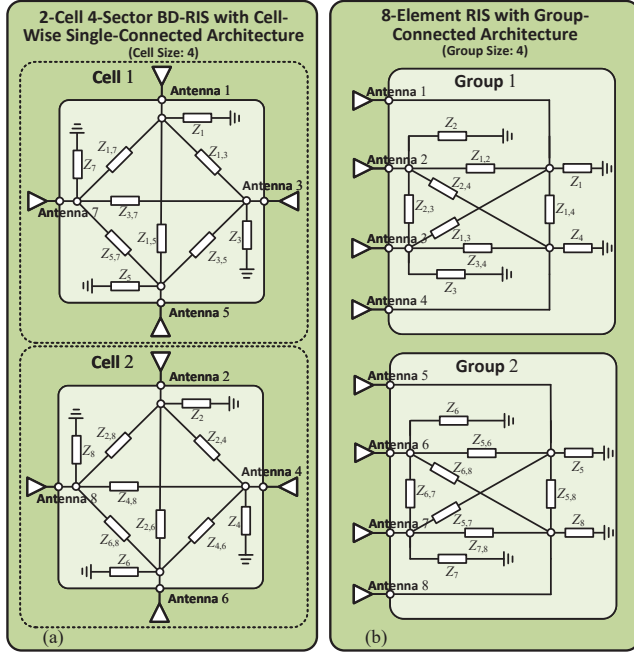


Fig. 5. Examples of (a) cell-wise single-connected multi-sector BD-RIS and (b) group-connected RIS in [22].

group-connected reconfigurable impedance network is utilized to support the multi-sector mode of the multi-sector BD-RIS, but to realize more flexible signal reflection for the group-connected RIS [22].

We model ϕ_i as $\phi_i = \sqrt{\beta_i}e^{j\vartheta_i}$, $\forall i \in \mathcal{L}_m$, $\forall m \in \mathcal{M}$, where $0 \leq \sqrt{\beta_i} \leq 1$ and $0 \leq \vartheta_i \leq 2\pi$ denote the amplitude and phase shift of ϕ_i , respectively. Next, we will consider two cases of the multi-sector BD-RIS: *i*) continuous case, that is both the amplitude and the phase shift have continuous values; *ii*) discrete case, that is both the amplitude and the phase shift are chosen from finite codebooks.

1) *Continuous Case*: In this case, constraint (8) is transformed into

$$(8) \Rightarrow \begin{cases} \phi_i = \sqrt{\beta_i}e^{j\vartheta_i}, \forall i \in \mathcal{L}_m, \forall m \in \mathcal{M}, \\ 0 \leq \beta_i \leq 1, \forall i \in \mathcal{L}_m, \forall m \in \mathcal{M}, \\ \sum_{i \in \mathcal{L}_m} \beta_i = 1, \forall m \in \mathcal{M}, \\ 0 \leq \vartheta_i < 2\pi, \forall i \in \mathcal{L}_m, \forall m \in \mathcal{M}. \end{cases} \quad (9)$$

2) *Discrete Case*: We propose a simple quantization strategy when ϕ_i has discrete values. Specifically, the amplitude square β_i is uniformly spaced within the range $[0, 1]$, i.e., $\beta_i \in \mathcal{A} = \{\frac{a}{2^A-1} | a = 0, 1, \dots, 2^A - 1\}$ controlled by A bits. The phase shift ϑ_i is uniformly spaced around the unit circle, i.e., $\vartheta_i \in \mathcal{B} = \{\frac{2\pi b}{2^B} | b = 0, 1, \dots, 2^B - 1\}$ controlled by B bits. In this case, constraint (8) is transformed into

$$(8) \Rightarrow \begin{cases} \phi_i = \sqrt{\beta_i}e^{j\vartheta_i}, \forall i \in \mathcal{L}_m, \forall m \in \mathcal{M}, \\ \beta_i \in \mathcal{A}, \forall i \in \mathcal{L}_m, \forall m \in \mathcal{M}, \\ \sum_{i \in \mathcal{L}_m} \beta_i = 1, \forall m \in \mathcal{M}, \\ \vartheta_i \in \mathcal{B}, \forall i \in \mathcal{L}_m, \forall m \in \mathcal{M}. \end{cases} \quad (10)$$

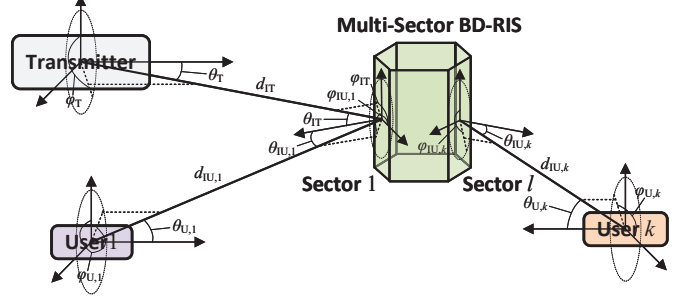


Fig. 6. Relative locations among the multi-sector BD-RIS, the transmitter, and users.

B. Channel Model

We start by analyzing the path loss of the multi-sector BD-RIS-assisted communication system, which will be used to model the multi-sector BD-RIS-assisted channel (5).

The relative locations among the transmitter, the multi-sector BD-RIS, and users are illustrated in Fig. 6. According to Friis transmission equation [28], the power captured by each antenna in sector 1 of the multi-sector BD-RIS from the transmitting antenna is¹

$$P_{IT} = \bar{P}_T \left(\frac{\lambda}{4\pi d_{IT}} \right)^2 G_T(\theta_T, \varphi_T) G_I(\theta_{IT}, \varphi_{IT}), \quad (11)$$

where \bar{P}_T is the power radiated from the transmitting antenna². $G_T(\theta_T, \varphi_T)$ ($G_I(\theta_{IT}, \varphi_{IT})$) is the gain of each transmitting antenna (each RIS antenna)³, where θ_T (θ_{IT}) and φ_T (φ_{IT}) are elevation and azimuth angles from the transmitter to sector 1 of the multi-sector BD-RIS (from sector 1 of the multi-sector BD-RIS to the transmitter), respectively. d_{IT} denotes the distance between the transmitter and the multi-sector BD-RIS. Then the power scattered from RIS antenna m , $\forall m \in \mathcal{M}_l$ in sector l , $\forall l \in \mathcal{L}$ can be represented as

$$P_{l,m} = P_{IT} |\phi_m|^2 = P_{IT} \beta_m, \forall m \in \mathcal{M}_l, \forall l \in \mathcal{L}. \quad (12)$$

Similarly, the power received by user k , $\forall k \in \mathcal{K}_l$ from RIS antenna m , $\forall m \in \mathcal{M}_l$ in sector l , $\forall l \in \mathcal{L}$ is given by

$$P_{U,m,k} = P_{l,m} \left(\frac{\lambda}{4\pi d_{IU,k}} \right)^2 G_I(\theta_{IU,k}, \varphi_{IU,k}) G_U(\theta_{U,k}, \varphi_{U,k}), \quad \forall m \in \mathcal{M}_l, \forall k \in \mathcal{K}_l, \forall l \in \mathcal{L}, \quad (13)$$

where $\theta_{IU,k}$ ($\theta_{U,k}$) and $\varphi_{IU,k}$ ($\varphi_{U,k}$) are elevation and azimuth angles from RIS antenna m to user k (from user k to RIS antenna m), respectively. $d_{IU,k}$ is the distance between the

¹In this paper, we consider a far-field case, that is the distance between the transmitter/users and the multi-sector BD-RIS is much larger than the size of the transmitter/RIS/users. In this case, we ignore the antenna spacing at the transmitter/RIS/users and the distance among different sectors of the multi-sector BD-RIS.

²We assume each transmitting antenna radiates the same power.

³We assume antennas at the transmitter/RIS/users have the same normalized power radiation pattern.

multi-sector BD-RIS and user k . Combining equations (11)–(13), we can obtain

$$P_{U,m,k} = \bar{P}_T \beta_m \frac{\lambda^4 G_T(\theta_T, \varphi_T) G_U(\theta_{U,k}, \varphi_{U,k})}{(4\pi)^4 (d_{IT} d_{IU,k})^2} \times G_I(\theta_{IT}, \varphi_{IT}) G_I(\theta_{IU,k}, \varphi_{IU,k}), \quad (14)$$

$$\forall m \in \mathcal{M}_l, \forall k \in \mathcal{K}_l, \forall l \in \mathcal{L}.$$

To separate factors related to the transmitter/users and to the multi-sector BD-RIS, and focus only on the impact from the multi-sector BD-RIS, we assume antennas at the transmitter/users exhibit constant gain, that is $G_T(\theta_T, \varphi_T) = G_T$ and $G_U(\theta_{U,k}, \varphi_{U,k}) = G_U$, $\forall k \in \mathcal{K}_l$, $\forall l \in \mathcal{L}$. Then with equation (14), we define the cascaded path loss of the multi-sector BD-RIS-assisted communication system as

$$\zeta_k = \frac{(4\pi)^4}{\lambda^4 G_T G_U} \frac{(d_{IT} d_{IU,k})^2}{G_I(\theta_{IT}, \varphi_{IT}) G_I(\theta_{IU,k}, \varphi_{IU,k})}, \quad (15)$$

$$\forall k \in \mathcal{K}_l, \forall l \in \mathcal{L}.$$

It can be observed from equation (15) that the path loss is highly associated with the gain of RIS antennas. In the following we will introduce two expressions of the gain of RIS antennas which are suitable for the multi-sector BD-RIS-assisted communication system.

1) *Idealized Radiation Pattern*: We first consider an idealized radiation pattern function for each antenna of the L -sector BD-RIS, which is given by

$$F_I^{\text{Idealized}}(\theta_I, \varphi_I) = \begin{cases} 1, & 0 \leq \theta_I \leq \frac{\pi}{L}, 0 \leq \varphi_I \leq 2\pi, \\ 0, & \frac{\pi}{L} < \theta_I \leq \pi, 0 \leq \varphi_I \leq 2\pi. \end{cases} \quad (16)$$

According to antenna theory [28], by assuming 100% radiation efficiency, i.e., $\eta = 1$, we can calculate the corresponding antenna gain as

$$G_I^{\text{Idealized}}(\theta_I, \varphi_I) = \begin{cases} \frac{2}{1 - \cos \frac{\pi}{L}}, & 0 \leq \theta_I \leq \frac{\pi}{L}, \\ 0, & \frac{\pi}{L} < \theta_I \leq \pi. \end{cases} \quad (17)$$

With $0 \leq \theta_{IT} \leq \frac{\pi}{L}$, and $0 \leq \theta_{IU,k} \leq \frac{\pi}{L}$, $\forall k \in \mathcal{K}_l$, $\forall l \in \mathcal{L}$, the corresponding path loss is given by

$$\zeta_k^{\text{Idealized}} = \frac{4^3 \pi^4 d_{IT}^2 d_{IU,k}^2 (1 - \cos \frac{\pi}{L})^2}{\lambda^4 G_T G_U}, \quad \forall k \in \mathcal{K}_l, \forall l \in \mathcal{L}. \quad (18)$$

2) *Practical Radiation Pattern*: We then choose a proper and popular radiation pattern function for each antenna of the L -sector BD-RIS, which is given by [28]

$$F_I^{\text{Practical}}(\theta_I, \varphi_I) = \begin{cases} \cos^{\alpha_L} \theta_I, & 0 \leq \theta_I \leq \frac{\pi}{2}, 0 \leq \varphi_I \leq 2\pi, \\ 0, & \frac{\pi}{2} < \theta_I \leq \pi, 0 \leq \varphi_I \leq 2\pi, \end{cases} \quad (19)$$

where $\alpha_L > 0$. Then we can obtain the half-power beamwidth (HPBW) of an L -sector BD-RIS by setting $F_I(\theta_I, \varphi_I) = 0.5$, which yields

$$\text{HPBW}_I^{\text{Practical}} = 2 \arccos \sqrt[4]{0.5} = 2\pi/L, \quad (20)$$

where α_L can be determined by solving the equation function $\arccos \sqrt[4]{0.5} = \pi/L$. The antenna gain with $\eta = 1$ is

$$G_I^{\text{Practical}}(\theta_I, \varphi_I) = \begin{cases} 2(\alpha_L + 1) \cos^{\alpha_L} \theta_I, & 0 \leq \theta_I \leq \frac{\pi}{2}, \\ 0, & \frac{\pi}{2} < \theta_I \leq \pi. \end{cases} \quad (21)$$

With $0 \leq \theta_{IT} \leq \frac{\pi}{L}$, and $0 \leq \theta_{IU,k} \leq \frac{\pi}{L}$, $\forall k \in \mathcal{K}_l$, $\forall l \in \mathcal{L}$, the path loss is given by

$$\zeta_k^{\text{Practical}} = \frac{4^3 \pi^4 d_{IT}^2 d_{IU,k}^2}{\lambda^4 G_T G_U (\alpha_L + 1)^2 \cos^{\alpha_L} \theta_{IT} \cos^{\alpha_L} \theta_{IU,k}}, \quad (22)$$

$$\forall k \in \mathcal{K}_l, \forall l \in \mathcal{L}.$$

With the path loss model (18) or (22), we can model the multi-sector BD-RIS-assisted channel \mathbf{H}_k (5) as a combination of large-scale and small-scale fading, i.e.,

$$\mathbf{H}_k = \sqrt{\zeta_k^{-1}} \tilde{\mathbf{H}}_{UI,k} \Phi_l \tilde{\mathbf{H}}_{IT}, \quad \forall k \in \mathcal{K}_l, \forall l \in \mathcal{L}, \quad (23)$$

where ζ_k , $\forall k \in \mathcal{K}_l$, $\forall l \in \mathcal{L}$ denote path loss components accounting for the large-scale fading. $\tilde{\mathbf{H}}_{UI,k}$ and $\tilde{\mathbf{H}}_{IT}$ refer to the small-scale fading, such as Rician fading, i.e.,

$$\tilde{\mathbf{H}}_{UI,k} = \sqrt{\frac{\kappa_{UI,k}}{\kappa_{UI,k} + 1}} \tilde{\mathbf{H}}_{UI,k}^{\text{LoS}}(\theta_{IU,k}, \varphi_{IU,k}, \theta_{U,k}, \varphi_{U,k}) + \sqrt{\frac{1}{\kappa_{UI,k} + 1}} \tilde{\mathbf{H}}_{UI,k}^{\text{NLoS}}, \quad \forall k \in \mathcal{K}_l, \forall l \in \mathcal{L}, \quad (24)$$

$$\tilde{\mathbf{H}}_{IT} = \sqrt{\frac{\kappa_{IT}}{\kappa_{IT} + 1}} \tilde{\mathbf{H}}_{IT}^{\text{LoS}}(\theta_{IT}, \varphi_{IT}, \theta_T, \varphi_T) + \sqrt{\frac{1}{\kappa_{IT} + 1}} \tilde{\mathbf{H}}_{IT}^{\text{NLoS}}, \quad (25)$$

where $\kappa_{UI,k}$, $\forall k \in \mathcal{K}_l$, $\forall l \in \mathcal{L}$, and κ_{IT} denote the Rician factor, channels with superscript “LoS” and “NLoS” refer to line-of-sight (LoS) and non-line-of-sight (NLoS) components, respectively.

Remark 3. There are threefold differences between STAR-RIS/IOS [25], [26] and the proposed multi-sector BD-RIS.

- STAR-RIS/IOS [25], [26] is a special instance of our proposed multi-sector BD-RIS with $L = 2$.
- Our model includes the effect of antenna beamwidth (and gain). Since the coverage of each sector of the multi-sector BD-RIS decreases with the growth of the number of sectors L , the antennas utilized to realize the multi-sector BD-RIS have narrower beamwidth, and thus higher gains. The antenna gain has a significant influence on the fading channels as analyzed in Section II-B and thus on the system performance as illustrated in Sections IV and V.
- The proposed model is built upon a group-connected reconfigurable impedance network [22], [28], which cannot be done with IOS/STAR-RIS modeling [25], [26] without a rigorous derivation based on network analysis theory.

Now with the channel model (23), together with the path loss model (18) or (22) and the small-scale fading model (24) and (25), and the cell-wise single-connected multi-sector BD-RIS model with continuous values (9) or discrete values (10), we finally establish the multi-sector BD-RIS-assisted communication model. In Sections III–VI, we will first discuss the potential applications of the multi-sector BD-RIS and then use this model to evaluate the performance of multi-sector BD-RIS-assisted communication systems.

III. POTENTIAL APPLICATIONS OF MULTI-SECTOR BD-RIS

In this section, we list several potential applications of our proposed multi-sector BD-RIS.

A. Millimeter Wave/Terahertz Communications

The need for more spectrum resources and higher frequency bands, such as millimeter wave or even higher Terahertz frequency bands, to cater to various emerging applications is one of important driving trends for 6G [2], [30]. Wireless communications on higher frequency bands usually suffer from higher spreading loss, have limited multi-path and high sparsity, and are vulnerable to blockages [30]. The proposed multi-sector BD-RIS is particularly useful for addressing the above issues. First, since the antennas utilized to realize the multi-sector BD-RIS have higher gains with the increase of the number of sectors L , the multi-sector BD-RIS is favorable to compensate for the high spreading loss for millimeter wave/Terahertz communications. Second, the beams of the multi-sector BD-RIS can be highly directional (with increasing L) to apply to millimeter wave/Terahertz communication systems with strong LoS channels. Third, different from conventional RIS with only half-space coverage, the multi-sector BD-RIS enables full-space coverage, which is helpful for the coverage extension (especially when there are multiple obstacles).

B. Cell-Free Networks

Cell-free networks are considered as a promising technique to satisfy the seamless connectivity and demanding coverage requirements for 6G [31]. Existing works have investigated the integration of conventional RISs (which can only reflect signals towards one side) and cell-free networks and shown the advantages of deploying RISs in cell-free networks [32], [33]. However, in conventional RIS-aided networks, usually multiple RISs should be deployed since each RIS has limited coverage, leading to complicated topology design problems for practical RIS deployments. The proposed multi-sector BD-RIS can simplify the deployment issue and provide additional benefits due to the following two reasons. First, since the multi-sector BD-RIS has full-space coverage, the locations of multi-sector BD-RISs can be more flexible compared to that of conventional ones. Specifically, when the number of sectors $L > 2$, the multi-sector BD-RIS has a more stable structure, which means the multi-sector BD-RIS can be flexibly deployed into different locations, while STAR-RIS ($L = 2$) usually needs to be attached to building surfaces. Second, with higher performance enhancement and wider coverage, the required number of multi-sector BD-RIS in cell-free networks can be much smaller, which will further facilitate the practical implementations.

IV. SCALING LAW

In this section, we analyze how the received power of the multi-sector BD-RIS-assisted system scales as a function of

the number of sectors L to show the benefit of the proposed multi-sector BD-RIS.

We consider a multi-sector BD-RIS-assisted SU-SISO system ($N = K = N_k = 1$) for simplicity. The single-antenna transmitter is allocated within the coverage of sector 1 of the multi-sector BD-RIS with $\theta_{\text{IT}} = 0$. The single-antenna user is randomly allocated around the multi-sector BD-RIS, e.g., within the coverage of sector l' , $\forall l' \in \mathcal{L}$. The transmitting symbol is $s \in \mathbb{C}$ with $\mathbb{E}\{|s|^2\} = 1$. According to equations (23) and (28), the received signal is expressed as

$$\begin{aligned} y &= \sqrt{P_{\text{T}}}\mathbf{h}_{\text{UI}}^H\Phi_{l'}\mathbf{h}_{\text{IT}}s + n \\ &= \sqrt{P_{\text{T}}\zeta^{-1}}\tilde{\mathbf{h}}_{\text{UI}}^H\Phi_{l'}\tilde{\mathbf{h}}_{\text{IT}}s + n, \end{aligned} \quad (26)$$

where P_{T} denotes the transmitting power, $\mathbf{h}_{\text{UI}} \in \mathbb{C}^M$ and $\mathbf{h}_{\text{IT}} \in \mathbb{C}^M$ denote channels from sector l' of the multi-sector BD-RIS to the user and from the transmitter to sector 1 of the multi-sector BD-RIS with small-scale fading components $\tilde{\mathbf{h}}_{\text{UI}}$ and $\tilde{\mathbf{h}}_{\text{IT}}$, respectively. ζ is the path loss and n is the noise. The received signal power at the user side is given by

$$P_{\text{U}} = \left| \sqrt{P_{\text{T}}\zeta^{-1}}\tilde{\mathbf{h}}_{\text{UI}}^H\Phi_{l'}\tilde{\mathbf{h}}_{\text{IT}} \right|^2 = P_{\text{T}}\zeta^{-1}|\tilde{\mathbf{h}}_{\text{UI}}^H\Phi_{l'}\tilde{\mathbf{h}}_{\text{IT}}|^2. \quad (27)$$

To achieve maximum received signal power, we assume that when the user is within the coverage of sector l' , $\forall l' \in \mathcal{L}$, the corresponding sector is activated. In this case, we have

$$\Phi_l = \begin{cases} \text{diag}(\phi_{(l-1)M+1}, \dots, \phi_{lM}), & l = l', \\ \mathbf{0}, & l \neq l', \end{cases} \quad (28)$$

with $|\phi_j| = 1, \forall j \in \mathcal{M}_{l'}$. Then, when $\phi_{(l'-1)M+m} = -\angle([\tilde{\mathbf{h}}_{\text{UI}}^H]_m[\tilde{\mathbf{h}}_{\text{IT}}]_m)$, $\forall m \in \mathcal{M}$, the received power is maximized to

$$P_{\text{U}}^{\max} = P_{\text{T}}\zeta^{-1} \left(\sum_{\forall m \in \mathcal{M}} |[\tilde{\mathbf{h}}_{\text{UI}}^H]_m[\tilde{\mathbf{h}}_{\text{IT}}]_m| \right)^2. \quad (29)$$

We assume $\tilde{\mathbf{h}}_{\text{UI}}$ and $\tilde{\mathbf{h}}_{\text{IT}}$ are line-of-sight (LoS) channels for simplicity, i.e., $\tilde{\mathbf{h}}_i = [e^{j\psi_{i,1}}, \dots, e^{j\psi_{i,M}}]^T$, $\forall i \in \{\text{UI}, \text{IT}\}$. Then with $\phi_{(l'-1)M+m} = \psi_{\text{UI},m} - \psi_{\text{IT},m}$, $\forall m \in \mathcal{M}$, we have the following maximized received power

$$P_{\text{U}}^{\max} = P_{\text{T}}\zeta^{-1}M^2. \quad (30)$$

It can be observed from equation (30) that with fixed P_{T} , the maximum received power is determined by the number of cells M and the path loss, both of which are highly associated with the number of sectors L . In the following, we will derive the relationship between the maximum received power and L by considering both idealized and practical radiation patterns as illustrated in Sec. II-B.

1) *Idealized Radiation Pattern:* In this case, the path loss is independent of the location of the user. Therefore, the maximum received signal power is given by

$$P_{\text{U}}^{\text{idealized}} = \frac{P_{\text{T}}M^2\lambda^4G_{\text{T}}G_{\text{U}}}{4^3\pi^4d_{\text{IT}}^2d_{\text{IU}}^2(1 - \cos\frac{\pi}{L})^2}, \quad (31)$$

where d_{IU} denotes the distance between the multi-sector BD-RIS and the user. From (31) we can deduce that the maximum received power is proportional to the number of sectors L ($L \geq 2$) when other terms in equation (31) are fixed. However, when

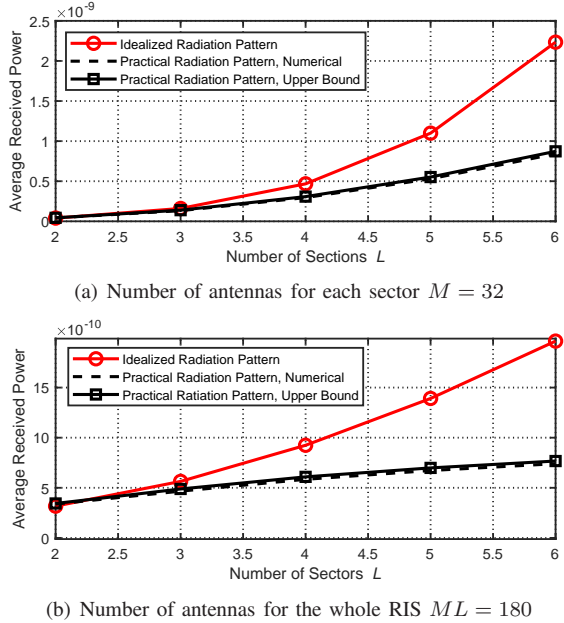


Fig. 7. Average received power versus the number of sectors L for the multi-sector BD-RIS. ($G_T = G_U = 1$, $P_T = 1$ W, $d_{IT} = 100$ m, $d_{IU} = 10$ m, $\lambda = c/f$ with $f = 2.4$ GHz.)

the number of antennas for the whole multi-sector BD-RIS is fixed, i.e., ML is fixed, the number of antennas for each sector M is inversely proportional to the number of sectors L . There might be a trade-off between M and L , which will be discussed in the following simulations.

2) *Practical Radiation Pattern*: The maximum received signal power with $\theta_{IT} = 0$ in this case is given by

$$P_U^{\text{Practical}} = \frac{P_T M^2 \lambda^4 G_T G_U}{4^3 \pi^4 d_{IT}^2 d_{IU}^2} (\alpha_L + 1)^2 \cos^{\alpha_L} \theta_{IU}. \quad (32)$$

Given that the user is randomly allocated around the multi-sector BD-RIS, we have $\theta_{IU} \sim \mathcal{U}(0, \pi/L)$. Therefore, the average of $P_U^{\text{Practical}}$ is given by

$$\begin{aligned} \bar{P}_U^{\text{Practical}} &= \mathbb{E}\{P_U^{\text{Practical}}\} \\ &= \frac{P_T M^2 \lambda^4 G_T G_U}{4^3 \pi^4 d_{IT}^2 d_{IU}^2} (\alpha_L + 1)^2 \mathbb{E}\{\cos^{\alpha_L} \theta_{IU}\} \\ &\leq \frac{P_T M^2 \lambda^4 G_T G_U}{4^3 \pi^4 d_{IT}^2 d_{IU}^2} (\alpha_L + 1)^2 \cos^{\alpha_L} \mathbb{E}\{\theta_{IU}\} \quad (33) \\ &= \frac{P_T M^2 \lambda^4 G_T G_U}{4^3 \pi^4 d_{IT}^2 d_{IU}^2} (\alpha_L + 1)^2 \cos^{\alpha_L} \frac{\pi}{2L} \\ &= \tilde{P}_U^{\text{Practical}}. \end{aligned}$$

From the relationship $\arccos \sqrt{0.5} = \pi/L$ we can obtain that the number of sectors L is proportional to α_L . In addition, with the growth of L , $\cos^{\alpha_L} \frac{\pi}{2L}$ is always within the range $0.5 < \cos^{\alpha_L} \frac{\pi}{2L} < 1$, while α_L grows significantly, such that $\tilde{P}_U^{\text{Practical}}$ is proportional to the number of sectors L (with fixed M). Similarly, when we fix the number of antennas ML for the whole multi-sector BD-RIS, the relationship between the maximum received power and the number of sectors L might not be that straightforward.

To clarify the relationship between the received power and the number of sectors L , in Fig. 7(a) we first plot the received power $P_U^{\text{Idealized}}$ using an idealized radiation pattern, $\bar{P}_U^{\text{Practical}}$ with a practical radiation pattern, and its upper bound $\tilde{P}_U^{\text{Practical}}$ versus the number of sectors L when the number of antennas for each sector is fixed to $M = 32$. It can be observed from Fig. 7 that the received power increase with the growth of L , and that $\bar{P}_U^{\text{Practical}}$ can finely approach its upper bound $\tilde{P}_U^{\text{Practical}}$. Then in Fig. 7(b), we plot the received power versus the number of sectors when the number of antennas for the whole multi-sector BD-RIS is fixed as $ML = 180$. In this case, the dimension of each sector of the multi-sector BD-RIS decreases with the growth of the number of sectors L . The received power still increases significantly, which indicates the impact of the antenna gain is more dominant than that of the dimension of RIS sectors. Based on the above analysis, the proposed multi-sector BD-RIS-assisted system is expected to achieve better performance when the number of sectors gets larger. To verify this conjecture, in the following section we will focus on the beamforming design to maximize the sum-rate performance for the multi-sector BD-RIS-assisted system.

V. BEAMFORMING DESIGN FOR MULTI-SECTOR BD-RIS-ASSISTED MU-MISO SYSTEM

In this section we apply the multi-sector BD-RIS in MU-MISO communication systems and propose efficient algorithms to design the multi-sector BD-RIS for both continuous and discrete cases.

A. Problem Formulation and Optimization Framework

We consider a multi-sector BD-RIS-assisted MU-MISO system ($N_k = 1, \forall k \in \mathcal{K}$) in accordance with Section III. The transmitting symbol vector is $\mathbf{s} \triangleq [s_1, \dots, s_K]^T \in \mathbb{C}^K$ with $\mathbb{E}\{\mathbf{s}\mathbf{s}^H\} = \mathbf{I}_K$. The transmitter applies a precoder matrix $\mathbf{W} \triangleq [\mathbf{w}_1, \dots, \mathbf{w}_K] \in \mathbb{C}^{N \times K}$ with $\mathbf{w}_k \in \mathbb{C}^N$ for user k , $\forall k \in \mathcal{K}$. With equations (5) and (7), the received signal y_k for user k is expressed as

$$\begin{aligned} y_k &= \mathbf{h}_{UI,k}^H \boldsymbol{\Phi}_l \mathbf{H}_{IT} \mathbf{W} \mathbf{s} + n_k, \\ &= \mathbf{v}_{k,k}^H \boldsymbol{\phi}_l s_k + \sum_{\substack{p \in \mathcal{K} \\ p \neq k}} \mathbf{v}_{k,p}^H \boldsymbol{\phi}_l s_p + n_k, \forall k \in \mathcal{K}, \forall l \in \mathcal{L}, \quad (34) \end{aligned}$$

where $\mathbf{v}_{k,p} = (\mathbf{h}_{UI,k}^H \text{diag}(\mathbf{H}_{IT} \mathbf{w}_p))^H$, $\forall p, k \in \mathcal{K}$, $\boldsymbol{\phi}_l = [\phi_{(l-1)M+1}, \dots, \phi_{lM}]^T$, $\forall l \in \mathcal{L}$, $\mathbf{h}_{UI,k} \in \mathbb{C}^M$, $\forall k \in \mathcal{K}$ is the channel vector between the multi-sector BD-RIS and user k , and $n_k \sim \mathcal{CN}(0, \sigma_k^2)$ is the noise. The sum-rate maximization problem can be formulated as

$$\max_{\mathbf{W}} \sum_{l \in \mathcal{L}} \sum_{k \in \mathcal{K}_l} \log_2 \left(1 + \frac{|\mathbf{v}_{k,k}^H \boldsymbol{\phi}_l|^2}{\sum_{\substack{p \in \mathcal{K} \\ p \neq k}} |\mathbf{v}_{k,p}^H \boldsymbol{\phi}_l|^2 + \sigma_k^2} \right) \quad (35a)$$

$$\text{s.t. (9) or (10),} \quad (35b)$$

$$\|\mathbf{W}\|_F^2 \leq P_T. \quad (35c)$$

Problem (35) is a typical sum-of-functions-of-ratio optimization, which can be solved by the general algorithm proposed in our previous work [27]. However, phase shifts and amplitudes

of non-zero multi-sector BD-RIS elements are partitioned based on the illustration in Section III, which will facilitate the multi-sector BD-RIS design. Therefore, in this work we follow the framework in [27], whose main idea is to first transform the original problem into a multi-block optimization and then iteratively design each block until convergence, but reconsider the design of the multi-sector BD-RIS block. Specifically, we first apply $2K$ auxiliary variables, ι_k and τ_k , $\forall k \in \mathcal{K}$, and transform (35) based on fractional programming theory [34] into the following four-block optimization:

$$\begin{aligned} & \max_{\mathbf{W}, \{\iota_k\}_{\forall k \in \mathcal{K}}, \{\tau_k\}_{\forall k \in \mathcal{K}}, \{\phi_l\}_{\forall l \in \mathcal{L}}} \sum_{l \in \mathcal{L}} \sum_{k \in \mathcal{K}_l} \left(\log_2(1 + \iota_k) - \iota_k + 2\sqrt{1 + \iota_k} \right. \\ & \quad \times \Re\{\tau_k^* \mathbf{v}_{k,k}^H \phi_l\} - |\tau_k|^2 \left(\sum_{p \in \mathcal{K}} |\mathbf{v}_{k,p}^H \phi_l|^2 + \sigma_k^2 \right) \left. \right) \\ & \text{s.t.} \quad (35b), (35c). \end{aligned} \quad (36)$$

Solutions to blocks $\{\iota_k\}_{\forall k \in \mathcal{K}}$, $\{\tau_k\}_{\forall k \in \mathcal{K}}$, and \mathbf{W} are similar to that in [27] with simple scaling of matrix dimensions, which are omitted due to the space limitation. In the following subsection, we will propose efficient algorithms to determine block $\{\phi_l\}_{\forall l \in \mathcal{L}}$ for both continuous and discrete cases.

B. Solution to $\{\phi_l\}_{\forall l \in \mathcal{L}}$

When blocks $\{\iota_k\}_{\forall k \in \mathcal{K}}$, $\{\tau_k\}_{\forall k \in \mathcal{K}}$, and \mathbf{W} are given, we can remove the constant terms in problem (36) and formulate the sub-problem with respect to $\{\phi_l\}_{\forall l \in \mathcal{L}}$ as

$$\begin{aligned} & \max_{\{\phi_l\}_{\forall l \in \mathcal{L}}} \sum_{l \in \mathcal{L}} \left(2\Re\{\tilde{\mathbf{v}}_l^H \phi_l\} - \phi_l^H \mathbf{V}_l \phi_l \right) \\ & \text{s.t.} \quad (35b), \end{aligned} \quad (37)$$

where $\tilde{\mathbf{v}}_l = (\sum_{k \in \mathcal{K}_l} \sqrt{1 + \iota_k} \tau_k^* \mathbf{v}_{k,k}^H)^H$, and $\mathbf{V}_l = \sum_{k \in \mathcal{K}_l} |\tau_k|^2 \sum_{p \in \mathcal{K}} \mathbf{v}_{k,p} \mathbf{v}_{k,p}^H$, $\forall l \in \mathcal{L}$. We successively design each cell of the multi-sector BD-RIS with fixed other cells until the convergence is guaranteed. Specifically, the sub-problem for the design of cell m , i.e., ϕ_i , $\forall i \in \mathcal{L}_m$ while fixing the rest of $M - 1$ cells is given by

$$\min_{\{\phi_i\}_{\forall i \in \mathcal{L}_m}} \sum_{i \in \mathcal{L}_m} \left(\nu_i |\phi_i|^2 + 2\Re\{\phi_i^* \chi_i\} \right) \quad (38a)$$

$$= \min_{\{\beta_i\}_{\forall i \in \mathcal{L}_m}} \sum_{i \in \mathcal{L}_m} \left(\nu_i \beta_i + 2|\chi_i| \sqrt{\beta_i} \cos(\angle \chi_i - \vartheta_i) \right) \quad (38b)$$

$$\text{s.t.} \quad (35b), \quad (38c)$$

where $\chi_{(l-1)M+m} = \sum_{n \neq m} [\mathbf{V}_l]_{m,n} \phi_{(l-1)M+n} - [\tilde{\mathbf{v}}_l]_m$, and $\nu_{(l-1)M+m} = [\mathbf{V}_l]_{m,m}$, $\forall l \in \mathcal{L}$, $\forall m \in \mathcal{M}$. In the following we will consider the phase shift and amplitude design for both continuous and discrete cases.

1) *Continuous Case with Constraint (9):* In this case, phase shifts ϑ_i , $\forall i \in \mathcal{L}_m$ can be easily obtained by setting $\cos(\angle \chi_i - \vartheta_i) = -1$, $\forall i \in \mathcal{L}_m$, which yields

$$\theta_i^* = \angle \chi_i \pm \pi, \forall i \in \mathcal{L}_m. \quad (39)$$

Substituting θ_i^* , $\forall i \in \mathcal{L}_m$ into objective (38b), we can obtain a real-value problem with respect to β_i , $\forall i \in \mathcal{L}_m$ as

$$\min_{\{\beta_i\}_{\forall i \in \mathcal{L}_m}} \sum_{i \in \mathcal{L}_m} \left(\nu_i \beta_i - 2|\chi_i| \sqrt{\beta_i} \right) = \min_{\beta_m} f(\beta_m) \quad (40a)$$

$$\text{s.t.} \quad 0 \leq \beta_i \leq 1, \forall i \in \mathcal{L}_m, \quad (40b)$$

$$\beta_m^T \beta_m = 1, \quad (40c)$$

where $f(\beta_m) = \beta_m^T \Psi_m \beta_m - 2\chi_m^T \beta_m$ with vector $\beta_m = [\sqrt{\beta_m}, \sqrt{\beta_{M+m}}, \dots, \sqrt{\beta_{(L-1)M+m}}]^T$, matrix $\Psi_m = \text{diag}(\nu_m, \nu_{M+m}, \dots, \nu_{(L-1)M+m})$, and vector $\chi_m = [|\chi_m|, |\chi_{M+m}|, \dots, |\chi_{(L-1)M+m}|]^T$. Since $|\chi_i| > 0$, $\forall i \in \mathcal{L}_m$, constraint (40b) can always be satisfied when problem (40) achieve its minimum. This observation motivates us to ignore constraint (40b), which yields

$$\beta_m^* = \arg \min_{\beta_m^T \beta_m = 1} f(\beta_m) \quad (41)$$

The optimal solution to problem (41) can be determined by the following lemma [35].

Lemma 1. β_m is the optimal solution to problem (41) if and only if there exists $\mu \in \mathbb{R}$ such that $(\Psi_m + \mu \mathbf{I}_L) \beta_m = \chi_m$, $\Psi_m + \mu \mathbf{I}_L$ positive semi-definite, and $\beta_m^T \beta_m = 1$.

Proof. By applying the Lagrange method, we can easily obtain $(\Psi_m + \mu \mathbf{I}_L) \beta_m = \chi_m$ with $\beta_m^T \beta_m = 1$, where $\mu \in \mathbb{R}$ is the Lagrange multiplier. Now it remains to show $\Psi_m + \mu \mathbf{I}_L$ is positive semi-definite. Suppose β_m' is a feasible solution of problem (41) with $\beta_m'^T \beta_m' = 1$. Then we have $f(\beta_m') \geq f(\beta_m^*)$. Given that $(\Psi_m + \mu \mathbf{I}_L) \beta_m^* = \chi_m$, we have

$$\begin{aligned} & \beta_m'^T \Psi_m \beta_m' - 2\beta_m'^T (\Psi_m + \mu \mathbf{I}_L) \beta_m' \\ & \geq \beta_m'^T \Psi_m \beta_m^* - 2\beta_m'^T (\Psi_m + \mu \mathbf{I}_L) \beta_m^*. \end{aligned} \quad (42)$$

Rearranging (42), we have

$$\begin{aligned} & (\beta_m'^T - \beta_m^T) (\Psi_m + \mu \mathbf{I}_L) (\beta_m' - \beta_m^*) \\ & \geq \mu (\beta_m'^T \beta_m' - \beta_m^T \beta_m^*) = 0, \end{aligned} \quad (43)$$

which completes the proof. \square

According to Lemma 1, β_m has a close-form solution as a function of μ , which is constrained by

$$\begin{aligned} g(\mu) &= \beta_m^T \beta_m^* = \chi_m^T (\Psi_m + \mu \mathbf{I}_L)^{-2} \chi_m \\ &= \text{Tr}\{(\Psi_m + \mu \mathbf{I}_L)^{-2} \chi_m \chi_m^T\} \\ &\stackrel{(a)}{=} \text{Tr}\{(\mathbf{U}_m \Sigma_m \mathbf{U}_m^T + \mu \mathbf{I}_L)^{-2} \chi_m \chi_m^T\} \\ &= \text{Tr}\{(\Sigma_m + \mu \mathbf{I}_L)^{-2} \mathbf{U}_m^T \chi_m \chi_m^T \mathbf{U}_m\} \\ &\stackrel{(b)}{=} \sum_{l \in \mathcal{L}} \frac{\tilde{\chi}_{m,l}^2}{(\varepsilon_{m,l} + \mu)^2} = 1, \end{aligned} \quad (44)$$

where (a) holds by performing the eigenvalue decomposition $\Psi_m = \mathbf{U}_m \Sigma_m \mathbf{U}_m^T$ with $\Sigma_m = \text{diag}(\varepsilon_{m,1}, \dots, \varepsilon_{m,L})$, $\varepsilon_{m,1} \leq \varepsilon_{m,2} \leq \dots \leq \varepsilon_{m,L}$, and $\mathbf{U}_m = [\mathbf{u}_{m,1}, \dots, \mathbf{u}_{m,L}]$; (b) holds by defining $\tilde{\chi}_{m,l} = \chi_m^T \mathbf{u}_{m,l}$, $\forall l \in \mathcal{L}$. Recall that $|\chi_i| > 0$, $\nu_i > 0$, $\forall i \in \mathcal{L}_m$. We have $\tilde{\chi}_{m,l} \neq 0$ and thus $\varepsilon_{m,l} + \mu \neq 0$. In addition, according to Lemma 1, $\Psi_m + \mu \mathbf{I}$ is positive semi-definite such that $\varepsilon_{m,l} + \mu \geq 0$. Therefore, the optimal value of μ should be chosen such that $\varepsilon_{m,l} + \mu > 0$, $\forall l \in \mathcal{L}$ and

$g(\mu) = 1$. In the following lemma, we derive the upper bound and lower bound of μ [35].

Lemma 2. Define $\mathcal{E} = \{l | \varepsilon_{m,l} = \varepsilon_{m,1}, \forall l \in \mathcal{L}\}$. The optimal solution of μ is chosen within the range $\sqrt{\sum_{\forall l \in \mathcal{E}} \tilde{\chi}_{m,l}^2} - \varepsilon_{m,1} \leq \mu \leq \|\chi_m\|_2 - \varepsilon_{m,1}$.

Proof. With $\varepsilon_{m,l} + \mu \geq \varepsilon_{m,1} + \mu > 0$, we have

$$\begin{aligned} 1 = g(\mu) &= \sum_{l \in \mathcal{L}} \frac{\tilde{\chi}_{m,l}^2}{(\varepsilon_{m,l} + \mu)^2} \\ &\leq \sum_{l \in \mathcal{L}} \frac{\tilde{\chi}_{m,l}^2}{(\varepsilon_{m,1} + \mu)^2} = \frac{\|\chi_m\|_2^2}{(\varepsilon_{m,1} + \mu)^2}, \end{aligned} \quad (45)$$

which yields $\mu \leq \|\chi_m\|_2 - \varepsilon_{m,1}$. Meanwhile, we have

$$\begin{aligned} 1 = g(\mu) &= \sum_{l \in \mathcal{L}} \frac{\tilde{\chi}_{m,l}^2}{(\varepsilon_{m,l} + \mu)^2} \\ &\geq \sum_{l \in \mathcal{E}} \frac{\tilde{\chi}_{m,l}^2}{(\varepsilon_{m,l} + \mu)^2} = \frac{\sum_{\forall l \in \mathcal{E}} \tilde{\chi}_{m,l}^2}{(\varepsilon_{m,1} + \mu)^2}, \end{aligned} \quad (46)$$

and thus $\mu \geq \sqrt{\sum_{\forall l \in \mathcal{E}} \tilde{\chi}_{m,l}^2} - \varepsilon_{m,1}$. \square

After determining the upper and lower bounds of μ according to Lemma 2, we can use efficient methods, such as bisection search, to find the optimal μ^* such that $g(\mu^*) = 1$. The optimal solution of problem (41) is given by

$$\boldsymbol{\beta}_m^* = (\boldsymbol{\Psi}_m + \mu^* \mathbf{I}_L)^{-1} \boldsymbol{\chi}_m. \quad (47)$$

Combining (39) and (47), we finally obtain the solution of problem (38) as $\phi_i^* = \sqrt{\beta_i^*} e^{j\vartheta_i^*}$, $\forall i \in \mathcal{L}_m$.

2) *Discrete Case with Constraint (10):* In this case, we first find the solution of phase shifts ϑ_i^* , $\forall i \in \mathcal{L}_m$ for continuous case by (39). Then we apply a simple quantization operation to obtain the discrete phase shifts as

$$\vartheta_i^* = \left\lceil \frac{\vartheta_i^*}{\Delta_B} \right\rceil \times \Delta_B, \forall i \in \mathcal{L}_m, \quad (48)$$

where $\Delta_B = \frac{2\pi}{2^B}$ denotes the resolution of phase shift and $\lceil \cdot \rceil$ denotes the rounding operation. Then we substitute (48) to problem (38), which yields

$$\beta_i^* = \arg \min_{\sum_{i \in \mathcal{L}_m} \beta_i = 1, \beta_i \in \mathcal{A}} \sum_{\forall i \in \mathcal{L}_m} f_i(\beta_i) \quad (49)$$

where $f_i(\beta_i) = \beta_i \nu_i + 2|\chi_i| \sqrt{\beta_i} \cos(\angle \chi_i - \vartheta_i^*)$, $\forall i \in \mathcal{L}_m$. Ignoring the discrete constraint and following the procedure for the design of continuous case, we can obtain the continuous solution β_i^* , $\forall i \in \mathcal{L}_m$, which is further quantized by

$$\beta_i^* = \left\lceil \frac{\beta_i^*}{\Delta_A} \right\rceil \times \Delta_A, \forall i \in \mathcal{L}_m, \quad (50)$$

where $\Delta_A = \frac{1}{2^{A-1}}$ denotes the resolution of amplitude square. It is worth noting that there is no guarantee of $\sum_{i \in \mathcal{L}_m} \beta_i^* = 1$. More specifically, we have $\sum_{i \in \mathcal{L}_m} \beta_i^* = 1 + \zeta \Delta_A$, $\zeta \in \mathbb{Z}$ due to the rounding operation. In the following, we will propose a simple yet efficient algorithm to adjust the quantization result (50) so that the constraint is satisfied. The proposed algorithm is described in Phases 1-3.

Phase 1: Let $\zeta = \frac{1 - \sum_{\forall i \in \mathcal{L}_m} \beta_i^*}{\Delta_A}$. If $\zeta = 0$, stop this procedure; if $\zeta > 0$, go to Step 2; otherwise, go to Step 3.

Phase 2: Set $\zeta' = 1$. In the ζ' -th loop, do the following procedures until $\zeta' > \zeta$: For $\forall i \in \mathcal{L}_m$, if $\beta_i^* < 1$, calculate $\delta_i = f_i(\beta_i^* + \Delta_A) - f_i(\beta_i^*)$; otherwise, set δ_i to a sufficient large number, e.g., ∞ . Then find i' such that $\delta_{i'} = \min_{\forall i \in \mathcal{L}_m} \delta_i$ and replace $\beta_{i'}^*$ with $\beta_{i'}^* + \Delta_A$. Update $\zeta' = \zeta' + 1$.

Phase 3: Set $\zeta' = 1$. In the ζ' -th loop, do the following procedures until $\zeta' > -\zeta$: For $\forall i \in \mathcal{L}_m$, if $\beta_i^* > 0$, calculate $\delta_i = f_i(\beta_i^* - \Delta_A) - f_i(\beta_i^*)$; otherwise, set δ_i to ∞ . Then find i' satisfying $\delta_{i'} = \min_{\forall i \in \mathcal{L}_m} \delta_i$ and replace $\beta_{i'}^*$ with $\beta_{i'}^* - \Delta_A$. Update $\zeta' = \zeta' + 1$.

After processing Phases 1-3, we can obtain the modified β_i^* , $\forall i \in \mathcal{L}_m$ satisfying the constraint $\sum_{\forall i \in \mathcal{L}_m} \beta_i^* = 1$, and the solution of problem (38) as $\phi_i^* = \sqrt{\beta_i^*} e^{j\vartheta_i^*}$, $\forall i \in \mathcal{L}_m$.

3) *Summary:* With solutions to sub-problem (38), the procedures of multi-sector BD-RIS design for continuous/discrete cases are summarized as following Steps 1-4:

Step 1: Calculate $\tilde{\mathbf{v}}_l = (\sum_{k \in \mathcal{K}_l} \sqrt{1 + \iota_k \tau_k^*} \mathbf{v}_{k,k}^H)^H$ and $\mathbf{V}_l = \sum_{k \in \mathcal{K}_l} |\tau_k|^2 \sum_{p \in \mathcal{K}} \mathbf{v}_{k,p} \mathbf{v}_{k,p}^H$, $\forall l \in \mathcal{L}$. Go to Step 2 for continuous case or Step 3 for discrete case.

Step 2: For continuous case, do Steps 2.1-2.3 with $\forall m \in \mathcal{M}$:

Step 2.1: Calculate χ_i in problem (38) and obtain $\theta_i^* = \angle \chi_i \pm \pi$, $\forall i \in \mathcal{L}_m$.

Step 2.2: Find μ_m^* by bisection search based on Lemma 2 such that $g(\mu_m^*) = 1$, and obtain $\beta_m^* = (\boldsymbol{\Psi}_m + \mu_m^* \mathbf{I}_L)^{-1} \boldsymbol{\chi}_m$.

Step 2.3: Update $\phi_i^* = \sqrt{\beta_i^*} e^{j\vartheta_i^*}$, $\forall i \in \mathcal{L}_m$.

Step 3: For discrete case, do Steps 3.1-3.4 with $\forall m \in \mathcal{M}$:

Step 3.1: Calculate χ_i in problem (38), obtain θ_i^* , $\forall i \in \mathcal{L}_m$ as in Step 2.1 and quantize θ_i^* by $\vartheta_i^* = \left\lceil \frac{\theta_i^*}{\Delta_B} \right\rceil \times \Delta_B$, $\forall i \in \mathcal{L}_m$.

Step 3.2: Obtain the continuous solution β_m^* of problem (50) as in Step 2.2 and quantize β_m^* by $\beta_i^* = \left\lceil \frac{\beta_i^*}{\Delta_A} \right\rceil \times \Delta_A$, $\forall i \in \mathcal{L}_m$.

Step 3.3: Execute Phases 1-3.

Step 3.4: Update $\phi_i^* = \sqrt{\beta_i^*} e^{j\vartheta_i^*}$, $\forall i \in \mathcal{L}_m$.

Step 4: Repeat Step 2 for continuous case or Step 3 for discrete case until the convergence of ϕ_i^* or ϕ_i^* , $\forall l \in \mathcal{L}$ is achieved.

VI. PERFORMANCE EVALUATION

In this section, we evaluate the performance of the multi-sector BD-RIS-assisted MU-MISO system. Channels from the transmitter to the RIS and from the multi-sector BD-RIS to users are modeled as the combination of the large-scale and the small-scale Rician fading as illustrated in Sec. II-B. Each sector of the multi-sector BD-RIS is an $M_x \times M_y$ uniform planar array (UPA) and the transmitter is an N -antenna uniform linear array (ULA) with half-wavelength antenna spacing. Antenna gains for transmitter antennas and user antennas are fixed to $G_T = G_U = 1$. The frequency of the transmit signal is set as $f = 2.4$ GHz. Distances between the transmitter and the multi-sector BD-RIS and between the multi-sector BD-RIS and users

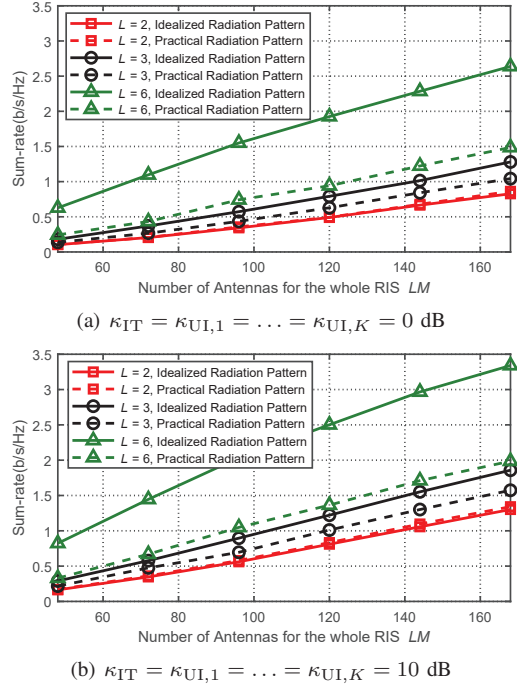


Fig. 8. Sum-rate versus the number of antennas for the whole multi-sector BD-RIS ($N = K = 6$, $M_y = 4$, $P_T = 10 \text{ dBm}$).

are $d_{TI} = 100 \text{ m}$ and $d_{IU,k} = 10 \text{ m}$, $\forall k \in \mathcal{K}$, respectively. The noise power is $\sigma_k^2 = -80 \text{ dBm}$, $\forall k \in \mathcal{K}$. In the following simulations, we assume K users are uniformly divided into L groups, each of which contains K/L users randomly located within the coverage of one sector.

Fig. 8 shows the sum-rate performance versus the number of antennas for the whole multi-sector BD-RIS. We consider different numbers of sectors and different Rician factors. We have the following observations from Fig. 8. *i*) Even with a reduced dimension for each sector, the sum-rate performance achieved by the multi-sector BD-RIS with an increasing number of sectors L still enhances, which is in accordance with the conclusion in Fig. 7(b). *ii*) Given the same fading conditions, the multi-sector BD-RIS with a smaller number of antennas but a larger number of sectors can achieve similar performance to that with a larger number of antennas but a smaller number of sectors. For example, when the practical radiation pattern is adopted, the sum-rate performance with $ML = 144$ and $L = 2$ is similar to that with $ML = 120$ and $L = 3$ as shown in Fig. 8(a). This phenomenon implies the number of antennas for the whole multi-sector BD-RIS can be reduced by increasing the number of sectors, which is meaningful for practical realizations of the multi-sector BD-RIS. *iii*) With the fixed number of sectors, the sum-rate performance based on the idealized radiation pattern is always at least equal to or better than that based on the practical radiation pattern, which, again, matches with the result in Fig. 7(b).

In Fig. 9 we plot the sum-rate performance as a function of the number of antennas for the whole multi-sector BD-RIS when each nonzero element of the multi-sector BD-RIS has discrete amplitudes and phase shifts controlled by different resolutions. Similar conclusions as Fig. 8 can be obtained from

Fig. 9. Moreover, we have the following additional observations. *i*) The sum-rate performance achieved by multi-sector BD-RIS with discrete values increases with the growth of resolutions. Specifically, when the idealized radiation pattern is applied for the modeling of fading channels, the sum-rate with $A = 3$ and $B = 3$ is close to that for the continuous case; when the practical radiation pattern is applied for the channel model, the sum-rate with $A = 2$ and $B = 2$ is sufficient to achieve satisfactory performance. *ii*) When the number of antennas for the whole RIS is fixed, the performance gap between RIS with different resolutions become smaller with the growth of the number of sectors L . Recalling that the sum-rate performance increases with L , we can deploy the multi-sector BD-RIS with a larger number of sectors and lower resolutions to achieve the same performance as that with a smaller number of sectors and higher resolution. For example, the sum-rate performance with $L = 3$, $A = B = 2$, and $M = 40$ in Fig. 9(b) is almost the same as that with $L = 6$, $A = B = 1$, and $M = 20$ in Fig. 9(f). Such reduction of resolutions is beneficial for reducing the cost of multi-sector BD-RIS realizations.

VII. CONCLUSION

In this paper, we propose a novel multi-sector BD-RIS model. Particularly, we derive the constraints of the cell-wise single-connected multi-sector BD-RIS for both continuous and discrete cases. We also derive the multi-sector BD-RIS-aided channel model including the impact of antenna gain. The existing STAR-RIS/IOS is a special instance of our proposed multi-sector BD-RIS model.

With the proposed model, we derive the scaling law of the received power as a function of the number of sectors for the multi-sector BD-RIS-aided SU-SISO system. We show that there is a positive correlation between the maximum received power and the number of sectors.

We then apply the multi-sector BD-RIS in the MU-MISO system and propose simple yet efficient algorithms to maximize the sum-rate of the multi-sector BD-RIS-aided MU-MISO system when amplitudes/phase shifts of the RIS have either continuous values or discrete values selected from finite codebooks. Simulation results show that given the same sum-rate requirement, the number of antennas for the whole multi-sector BD-RIS can be reduced by increasing the number of sectors, and that the codebook resolutions can also be reduced by increasing the number of sectors.

Based on the proposed multi-sector BD-RIS, there are many open problems worth being investigated in the near future, such as the modeling and design of cell-wise group/fully-connected multi-sector BD-RIS, and the integration of multi-sector BD-RIS with other promising techniques, such as ISAC, WPT, and RSMA.

REFERENCES

- [1] H. Tataria, M. Shafi, A. F. Molisch, M. Dohler, H. Sjöland, and F. Tufvesson, "6G wireless systems: Vision, requirements, challenges, insights, and opportunities," *Proceedings of the IEEE*, vol. 109, no. 7, pp. 1166–1199, 2021.
- [2] W. Saad, M. Bennis, and M. Chen, "A vision of 6G wireless systems: Applications, trends, technologies, and open research problems," *IEEE network*, vol. 34, no. 3, pp. 134–142, 2019.

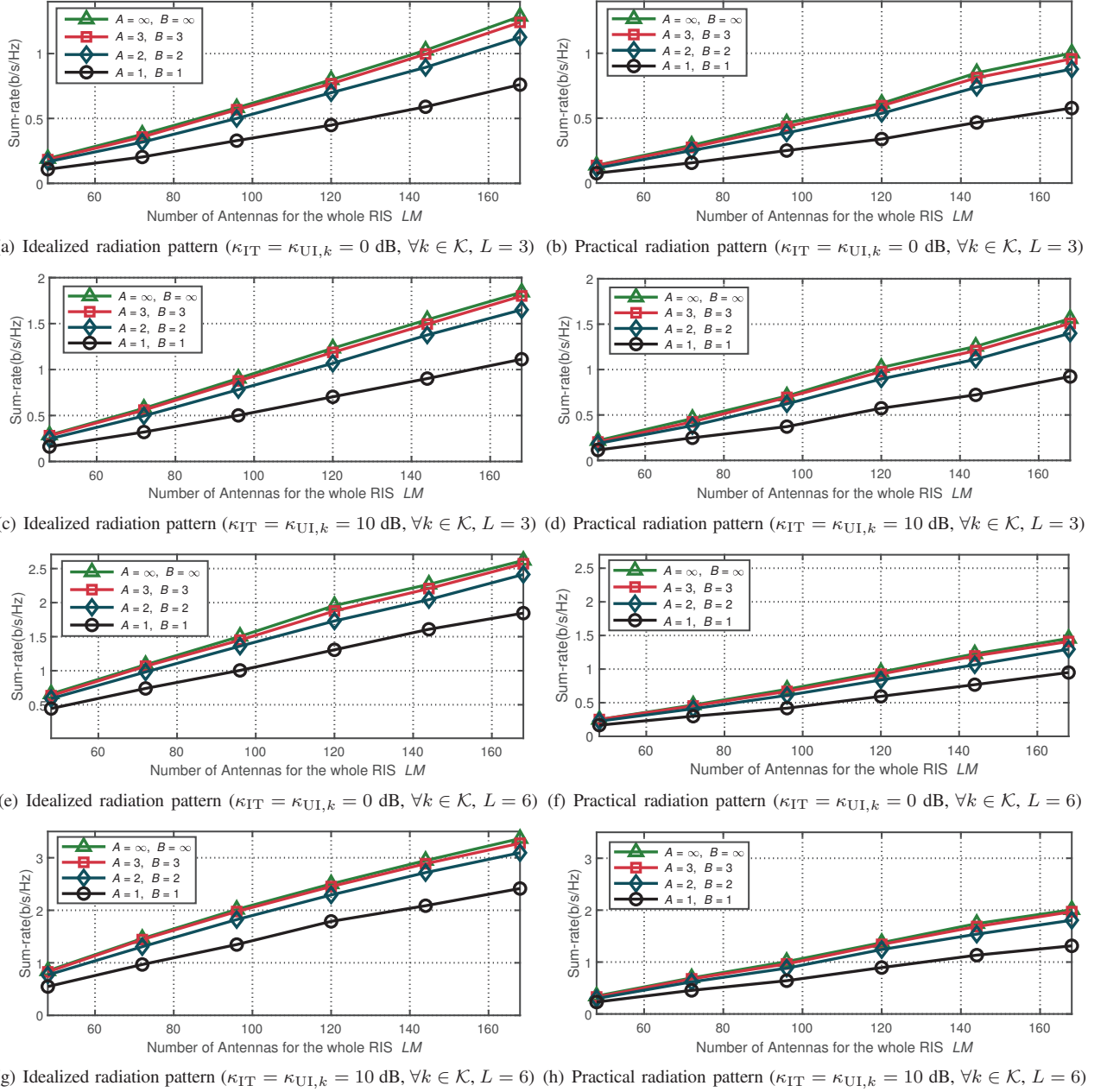


Fig. 9. Sum-rate versus the number of antennas for the whole multi-sector BD-RIS with different resolutions for amplitudes and phase shifts, different numbers of sectors, and different Rician fading factors ($N = K = 6$, $M_y = 4$, $P_T = 10$ dBm).

- [3] M. Di Renzo, A. Zappone, M. Debbah, M.-S. Alouini, C. Yuen, J. De Rosny, and S. Tretyakov, "Smart radio environments empowered by reconfigurable intelligent surfaces: How it works, state of research, and the road ahead," *IEEE Journal on Selected Areas in Communications*, vol. 38, no. 11, pp. 2450–2525, 2020.
- [4] M. Di Renzo, M. Debbah, D.-T. Phan-Huy, A. Zappone, M.-S. Alouini, C. Yuen, V. Sciancalepore, G. C. Alexandropoulos, J. Hoydis, H. Gacanin *et al.*, "Smart radio environments empowered by reconfigurable AI meta-surfaces: An idea whose time has come," *EURASIP Journal on Wireless Communications and Networking*, vol. 2019, no. 1, pp. 1–20, 2019.
- [5] H. Guo, Y.-C. Liang, J. Chen, and E. G. Larsson, "Weighted sum-rate maximization for reconfigurable intelligent surface aided wireless networks," *IEEE Transactions on Wireless Communications*, vol. 19, no. 5, pp. 3064–3076, 2020.
- [6] B. Di, H. Zhang, L. Song, Y. Li, Z. Han, and H. V. Poor, "Hybrid beamforming for reconfigurable intelligent surface based multi-user communications: Achievable rates with limited discrete phase shifts," *IEEE Journal on Selected Areas in Communications*, vol. 38, no. 8, pp. 1809–1822, 2020.
- [7] C. Huang, A. Zappone, G. C. Alexandropoulos, M. Debbah, and C. Yuen, "Reconfigurable intelligent surfaces for energy efficiency in wireless communication," *IEEE Transactions on Wireless Communications*, vol. 18, no. 8, pp. 4157–4170, 2019.
- [8] Q. Wu and R. Zhang, "Intelligent reflecting surface enhanced wireless network via joint active and passive beamforming," *IEEE Transactions on Wireless Communications*, vol. 18, no. 11, pp. 5394–5409, 2019.
- [9] ———, "Beamforming optimization for wireless network aided by intelligent reflecting surface with discrete phase shifts," *IEEE Transactions on Communications*, vol. 68, no. 3, pp. 1838–1851, 2019.
- [10] B. Zheng, C. You, and R. Zhang, "Double-IRS assisted multi-user mimo: Cooperative passive beamforming design," *IEEE Transactions on Wireless Communications*, vol. 20, no. 7, pp. 4513–4526, 2021.
- [11] A. Bansal, K. Singh, B. Clerckx, C.-P. Li, and M.-S. Alouini, "Rate-splitting multiple access for intelligent reflecting surface aided multi-user communications," *IEEE Transactions on Vehicular Technology*, vol. 70,

no. 9, pp. 9217–9229, 2021.

[12] Z. Feng, B. Clerckx, and Y. Zhao, “Waveform and beamforming design for intelligent reflecting surface aided wireless power transfer: Single-user and multi-user solutions,” *IEEE Transactions on Wireless Communications*, 2022.

[13] Y. Zhao, B. Clerckx, and Z. Feng, “IRS-aided SWIPT: Joint waveform, active and passive beamforming design under nonlinear harvester model,” *IEEE Transactions on Communications*, vol. 70, no. 2, pp. 1345–1359, 2021.

[14] R. Liu, M. Li, Y. Liu, Q. Wu, and Q. Liu, “Joint transmit waveform and passive beamforming design for RIS-aided DFRC systems,” *IEEE Journal of Selected Topics in Signal Processing*, 2022.

[15] D. Xu, X. Yu, Y. Sun, D. W. K. Ng, and R. Schober, “Resource allocation for IRS-assisted full-duplex cognitive radio systems,” *IEEE Transactions on Communications*, vol. 68, no. 12, pp. 7376–7394, 2020.

[16] S. Gopi, S. Kalyani, and L. Hanzo, “Intelligent reflecting surface assisted beam index-modulation for millimeter wave communication,” *IEEE Transactions on Wireless Communications*, vol. 20, no. 2, pp. 983–996, 2020.

[17] S. Abeywickrama, R. Zhang, Q. Wu, and C. Yuen, “Intelligent reflecting surface: Practical phase shift model and beamforming optimization,” *IEEE Transactions on Communications*, vol. 68, no. 9, pp. 5849–5863, 2020.

[18] W. Cai, H. Li, M. Li, and Q. Liu, “Practical modeling and beamforming for intelligent reflecting surface aided wideband systems,” *IEEE Communications Letters*, vol. 24, no. 7, pp. 1568–1571, 2020.

[19] H. Li, W. Cai, Y. Liu, M. Li, Q. Liu, and Q. Wu, “Intelligent reflecting surface enhanced wideband MIMO-OFDM communications: From practical model to reflection optimization,” *IEEE Transactions on Communications*, vol. 69, no. 7, pp. 4807–4820, 2021.

[20] Ö. Özdogan, E. Björnson, and E. G. Larsson, “Intelligent reflecting surfaces: Physics, propagation, and pathloss modeling,” *IEEE Wireless Communications Letters*, vol. 9, no. 5, pp. 581–585, 2019.

[21] W. Tang, M. Z. Chen, X. Chen, J. Y. Dai, Y. Han, M. Di Renzo, Y. Zeng, S. Jin, Q. Cheng, and T. J. Cui, “Wireless communications with reconfigurable intelligent surface: Path loss modeling and experimental measurement,” *IEEE Transactions on Wireless Communications*, vol. 20, no. 1, pp. 421–439, 2020.

[22] S. Shen, B. Clerckx, and R. Murch, “Modeling and architecture design of reconfigurable intelligent surfaces using scattering parameter network analysis,” *IEEE Transactions on Wireless Communications*, vol. 21, no. 2, pp. 1229–1243, 2021.

[23] M. Nerini and B. Clerckx, “Reconfigurable intelligent surfaces based on single, group, and fully connected discrete-value impedance networks,” *arXiv preprint arXiv:2110.00077*, 2021.

[24] Q. Li, M. El-Hajjar, I. A. Hemadeh, A. Shojaeifard, A. Mourad, B. Clerckx, and L. Hanzo, “Reconfigurable intelligent surfaces relying on non-diagonal phase shift matrices,” *IEEE Transactions on Vehicular Technology*, 2022.

[25] J. Xu, Y. Liu, X. Mu, and O. A. Dobre, “STAR-RISs: Simultaneous transmitting and reflecting reconfigurable intelligent surfaces,” *IEEE Communications Letters*, vol. 25, no. 9, pp. 3134–3138, 2021.

[26] H. Zhang, S. Zeng, B. Di, Y. Tan, M. Di Renzo, M. Debbah, Z. Han, H. V. Poor, and L. Song, “Intelligent omni-surfaces for full-dimensional wireless communications: Principles, technology, and implementation,” *IEEE Communications Magazine*, vol. 60, no. 2, pp. 39–45, 2022.

[27] H. Li, S. Shen, and B. Clerckx, “Beyond diagonal reconfigurable intelligent surfaces: From transmitting and reflecting modes to single-, group-, and fully-connected architectures,” *arXiv preprint arXiv:2205.02866v2*, 2022.

[28] C. A. Balanis, *Antenna theory: analysis and design*. John Wiley & Sons, 2015.

[29] D. M. Pozar, *Microwave engineering*. John Wiley & Sons, 2011.

[30] I. F. Akyildiz, C. Han, Z. Hu, S. Nie, and J. M. Jornet, “Terahertz band communication: An old problem revisited and research directions for the next decade,” *IEEE Transactions on Communications*, 2022.

[31] H. Q. Ngo, A. Ashikhmin, H. Yang, E. G. Larsson, and T. L. Marzetta, “Cell-free massive MIMO versus small cells,” *IEEE Transactions on Wireless Communications*, vol. 16, no. 3, pp. 1834–1850, 2017.

[32] Q. N. Le, V.-D. Nguyen, O. A. Dobre, and R. Zhao, “Energy efficiency maximization in RIS-aided cell-free network with limited backhaul,” *IEEE Communications Letters*, vol. 25, no. 6, pp. 1974–1978, 2021.

[33] T. Van Chien, H. Q. Ngo, S. Chatzinotas, M. Di Renzo, and B. Ottersten, “RIS and cell-free massive MIMO: A marriage for harsh propagation environments,” in *2021 IEEE Global Communications Conference (GLOBECOM)*. IEEE, 2021, pp. 01–06.

[34] K. Shen and W. Yu, “Fractional programming for communication systems—Part I: Power control and beamforming,” *IEEE Transactions on Signal Processing*, vol. 66, no. 10, pp. 2616–2630, 2018.

[35] W. W. Hager, “Minimizing a quadratic over a sphere,” *SIAM Journal on Optimization*, vol. 12, no. 1, pp. 188–208, 2001.